ADVANCED OPTICAL MATERIALS
www.advopticalmat.de

Optical Vortices Generation via a Self-Assembly Photonic Crystal Slab

Wenjie Zhang, Jiao Chu, Ruhuan Deng, Xinhao Wang, Tongyu Li, Wenzhe Liu, Jiajun Wang, Xiaohan Liu, and Lei Shi**

Optical vortices (OVs), as common phenomena that widely exist in nature, have attracted interest both in fundamental science and applications. Recently, generating OVs by using polarization vortices in the momentum space is demonstrated. This method eliminates the need for precise optical center alignment, which relies on periodic structures. The micro-spheres self-assembly method is known as an inexpensive and straightforward means to fabricate periodic structures. Here, self-assembly photonic crystal (SA-PhC) slabs are proposed that can be used to generate OVs. With both simulations and experiments, the OVs generation via SA-PhC slabs is investigated. The designed SA-PhC slab is fabricated. The momentum-space polarization vortex of the SA-PhC slab is directly observed. The field shape and phase distribution of the generated OVs are measured. The work can broaden the applications of SA-PhC and the generation methods of OVs.

1. Introduction

Optical vortices (OVs) are light with spiral wave fronts and central zero-intensity points.[1,2] The recent emergence of OVs leads to promising applications of integrated photonics and mode-division multiplexing,[3–5] optical communication,[6] optical particle manipulation,[7–10] optical microscopy,[11] and spin-orbit interactions of light,[12] etc. In order to generate OVs, various methods have been proposed such as spiral phase plates, Q plates and metasurfaces, etc.[13,14] In spiral phase plates, an axial phase difference is created by a medium of a radially varying thickness, and then OVs are generated.[15,16] In Q-plates, a cross-polarized circularly polarized transmitted light gains the Pancharatnam–Berry (PB) phase with a gradient along the axial direction.[17] This process transforms plane waves into OVs. And metasurfaces can introduce spiral phase wave fronts by space-variant subwavelength nanostructures.[18,19] These methods can generate OVs suitable for different applications. Nevertheless, a common challenge in all these methods is the inevitably precise optical center alignment. In recent years, a new method utilizing momentum-space vortices around bound states in the continuum (BICs)[20] to generate OVs was proposed and demonstrated, which eliminates the necessity for precise optical center alignment.[21] In this method, the winding topological polarization vortices exist in the photonic bands of photonic crystal (PhC) slabs.[22] When a circularly polarized light beam shines on the PhC slab, the cross-polarized light beam will obtain a polarization-dependent spiral phase vortice. The PhC slabs are periodic, without a real-space center. Hence the optical center alignment is not required. To obtain the periodic structures with required polarization vortices in momentum space, the electron beam lithography processes are usually applied, which are expensive and complicated. To promote the development and application of this OVs generation method, it is important to search for more methods to obtain periodic structures with momentum-space polarization vortices.

The micro-spheres self-assembly method could be promising, which is usually known as an inexpensive and straightforward means to fabricate PhC structures.[23] Initially, the periodic structures constructed by self-assembly micro-spheres were initially employed in 3D PhCs.[24,25] These PhCs found applications in structural coloration,[26–29] photonic bandgap,[30] and sensor.[31] Later, self-assembly of single-layer periodic arrays was developed,[32] and it could be used to fabricate 2D PhC slabs. These single-layer periodic arrays can be used to construct various complex nanostructures.[33–35] By placing these substrates on

W. Zhang, J. Chu, R. Deng, X. Wang, T. Li, J. Wang, X. Liu, L. Shi
State Key Laboratory of Surface Physics
Key Laboratory of Micro- and Nano-Photonic Structures (Ministry of Education) and Department of Physics
Fudan University
Shanghai 200433, China
E-mail: jiajunwang@fudan.edu.cn; lshi@fudan.edu.cn
W. Liu
Department of Physics
The Hong Kong University of Science and Technology
Hong Kong 999077, China
L. Shi
Institute for Nanoelectronic devices and Quantum computing
Fudan University
Shanghai 200438, China
L. Shi
Collaborative Innovation Center of Advanced Microstructures
Nanjing University
Nanjing 210093, China
L. Shi
Shanghai Research Center for Quantum Sciences
Shanghai 201315, China

The ORCID identification number(s) for the author(s) of this article can be found under https://doi.org/10.1002/adom.202400088

DOI: 10.1002/adom.202400088

the metal substrate, clear photonic bands have been observed and explored with applications like directional emission.[36–39] However, to date, the momentum-space polarization vortice and its application of OVs generation have never been explored in these self-assembly PhC (SA-PhC) slabs.

In this paper, we report the OVs generation via SA-PhC slabs, constructed by self-assembly polystyrene (PS) micro-spheres arrays on the Ag substrate. We theoretically and experimentally investigate the generation of OVs via momentum-space polarization vortices around at-Γ degenerate points. The SA-PhC slab was designed and optimized by changing the diameter of PS micro-spheres and the thickness of a SiO_2 layer between the PS micro-spheres arrays and the Ag substrate. The momentum-space polarization vortex around the degenerated points was measured. And OVs generation via the fabricated SA-PhC slab was directly measured.

2. Basic Principle and Sample Design

For the PhC slabs with high rotational symmetry, there are various momentum-space polarization vortices centered at Γ point. Such polarization vortices are symmetry-protected, which are independent of structure or material parameters. Hence, we can expect them in any PhC slabs with enough rotational symmetry. The momentum-space polarization vortice can carry topological charge q, which is defined by the winding number of the polarization axis around the vortice center:[40]

$$q = \frac{1}{2\pi}\oint_C \mathrm{d}k_{\parallel} \cdot \nabla_{k_{\parallel}}\theta(k_{\parallel}) \tag{1}$$

Here, the θ is the orientation of the major axis of the polarization state. For example, the right panel of **Figure 1a** exhibits a schematic polarization vortice that can exist in the SA-PhC slab. In our previous work, by considering the circularly polarized incidence, we have shown the ability of momentum-space polarization vortice to realize vortice phase for the cross-polarized light beam.[21] When a light beam shines on the PhC slab, it would interact with the optical modes. To discuss the interactions between the light beam and the optical modes in the polarization vortice, we can think about this process from the momentum space, i.e., the light beam is combined by a series of plane waves with different $k_{\parallel}$ ($k_{\parallel}$ is the projected wave vector in the plane perpendicular to the propagation axis of light beams). For each component of certain $k_{\parallel}$, they can interact with optical modes with the same $k_{\parallel}$, then the corresponding reflection or transmission will gain a phase modulation. We can formulate this process on a helical basis, and the reflection can be written as:[21,41]

$$|E_{out}\rangle = \begin{pmatrix} r_{ll} & r_{lr}e^{2i\theta(k_{\parallel})} \\ r_{rl}e^{-2i\theta(k_{\parallel})} & r_{rr} \end{pmatrix} |E_{in}\rangle \tag{2}$$

Here, $\theta(k_{\parallel})$ is the polarization orientation of the optical mode and r_{ll}, r_{lr}, r_{rl}, r_{rr} are the reflection coefficients. In this helical basis, the left- and right-handed circularly polarized unit vectors ($|L\rangle$ and $|R\rangle$) are $(1, 0)^T$ and $(0, 1)^T$ respectively. We can see that the cross-polarized components, i.e., the off-diagonal elements, have polarization-orientation-related geometric phase factors (also called the PB phase). For example, choosing the incident polarization to be left-handed circularly polarized, the reflection can be written as:

$$|E_{out}\rangle = r_{rl}e^{-2i\theta}\langle L||E_{in}\rangle|R\rangle + r_{ll}\langle L||E_{in}\rangle|L\rangle \tag{3}$$

Considering the existence of polarization vortice, we can know the cross-polarized left-handed circularly polarized light will gain a winding phase in momentum space. It is worth noting that in previous studies, polarization vortices applied for OV generation were mostly carried by BICs. In fact, besides BICs, the degenerate points at Γ point can also carry polarization vortice, while the corresponding application for OV generation has not been realized. In this work, we aim to utilize the polarization vortice around degenerate points at Γ point to realize OV generation.

To start, we consider a SA-PhC slab constructed by PS micro-spheres arrays on the Ag substrate. As is shown in the left panel of Figure 1a, the self-assembly PS micro-spheres are usually formed as a C_{6v} lattice. The period a is 700 nm, which is equal to the diameter of the PS micro-sphere. Figure 1b exhibits simulated angle-resolved reflectance spectra along the M and K direction. Figure 1c shows the corresponding cross-polarized conversion efficiency under circularly polarized incidence. It can be observed that there is a degenerate state at Γ point, as is marked by the red arrow in Figure 1b. It corresponds to the position with zero conversion efficiency in Figure 1c. Figure 1d shows the simulated cross-polarization phase distribution under left circularly polarized (LCP) incidence at a wavelength of 760 nm. It could be seen there is a spiral phase distribution with a +2 topological charge. Figure 1e shows conversion efficiency at a wavelength of 760 nm. It is a doughnut-shaped profile with central zero-intensity points, a key characteristic of OVs. Note that for this SA-PhC slab design, the cross-polarized conversion efficiency is relatively small.

Figure 1f shows the schematics of the optimized design SA-PhC slab. An additional SiO_2 spacer is included between the Ag substrate and the PS sphere to reduce the absorption, and the diameter of the sphere is reduced to increase the scattering efficiency.[41] The diameter d of the PS micro-spheres is reduced to 500 nm and the thickness h of the SiO_2 layer is 200 nm while the period is still 700 nm. Figure 1g exhibits simulated angle-resolved reflectance spectra along the Γ-M and Γ-K direction. Figure 1h shows the corresponding cross-polarized conversion efficiency under circularly polarized incidence. The degenerate point at Γ point is marked by the red arrow in Figure 1g, corresponding to a zero-conversion-efficiency position in Figure 1h. Figure 1i exhibits the simulated cross-polarization phase distribution under LCP incidence at a wavelength of 727 nm, showing spiral phase distribution with a +2 topological charge. Figure 1j shows conversion efficiency at a wavelength of 727 nm. In contrast with Figure 1e, the conversion efficiency is greatly improved in this optimized design.

3. Results and Discussion

Figure 2a shows the fabrication process. A 300-nm-thickness film and a 200-nm-thickness SiO_2 film are coated on a glass substrate by using electron beam evaporation. Figure 2b shows scanning electron microscope (SEM) pictures of the substrate cross-section corresponding to the fabrication process in Figure 2a. Next, self-assembly PS micro-spheres are arrayed on the SiO_2

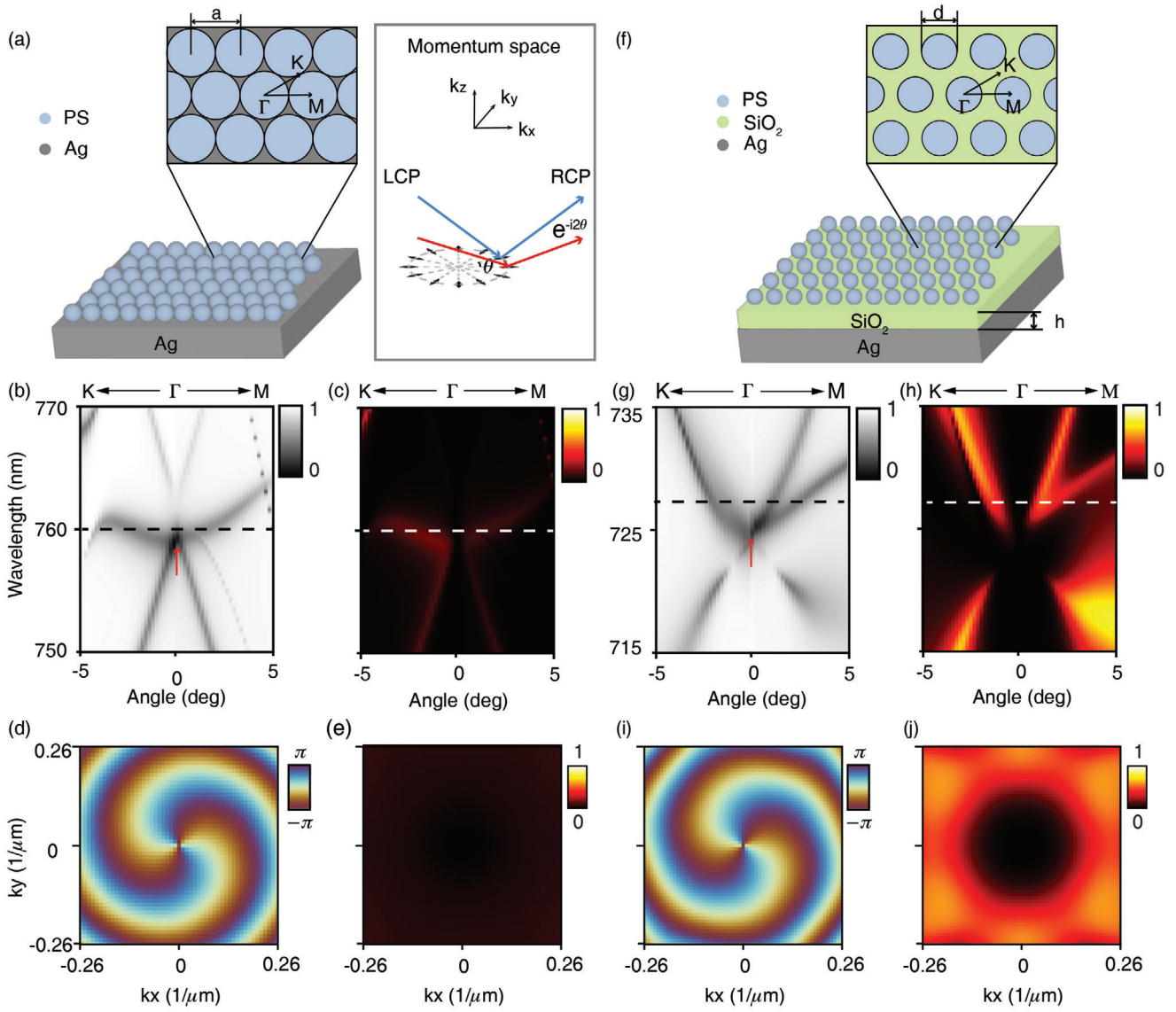

Figure 1. a) Left panel, a schematic of self-assembly PhC (SA-PhC) slab, constructed by PS micro-spheres arrayed in a hexagonal close-packing on an Ag film. The period *a* is 700 nm, which is equal to the diameter of the micro-spheres. Γ-M and Γ-K are two high symmetry directions. Right panel, a schematic of a polarization vortice existing in the SA-PhC slab. The black arrow represents the major axis of the polarization state, θ represents the orientation of the major axis of the polarization state, and the cross-polarized circularly polarized light will gain a winding phase in momentum space. The blue and red arrows represent different wave vectors (propagation directions), and they will excite different polarization states around Γ in momentum space, respectively. b,c) Simulated angle-resolved reflection spectra and conversion efficiency along high-symmetry directions. d,e) The momentum-space phase distribution and conversion efficiency of the cross-polarized light when a 760-nm circularly-polarized incidence is considered. f) Schematic showing optimized PS micro-spheres array. Schematic of optimized SA-PhC slab. The period is unchanged, while the diameter *d* of PS micro-sphere is shrunk to be 500 nm. And a 200-nm-thick SiO_2 spacer is added between the PS micro- spheres and the Ag substrate. g,h) Simulated angle-resolved reflection spectra and conversion efficiency for the optimized structures in (f). i,j) The momentum-space phase distribution and conversion efficiency of the cross-polarized light when a 727-nm circularly-polarized incidence is considered.

film, and they are arrayed in a hexagonal close-packing. Then, the diameter of PS micro-spheres is reduced by using reactive ion etching (RIE). Figure 2c shows SEM pictures of the self-assembled PS micro-spheres arrays. Before using RIE etching, the PS micro-spheres are arranged in a hexagonal lattice, while the period is equal to the diameter of the PS micro-spheres of 700 nm, after using RIE etching, the diameter of the PS micro-spheres is reduced to 500 nm.

Next, we measure the angle-resolved reflectance spectra and conversion efficiency (see Experimental and Computational Section for more details). **Figure** 3a,b show the angle-resolved reflectance spectra and conversion efficiency spectra along Γ-M and Γ-K. To demonstrate the vortice behavior of states of polarization (SOPs) around the Γ point, we conduct measurements of the polarization-dependent reflection iso-frequency contours at a central wavelength of 725 nm by a filter, whose bandwidth is 10

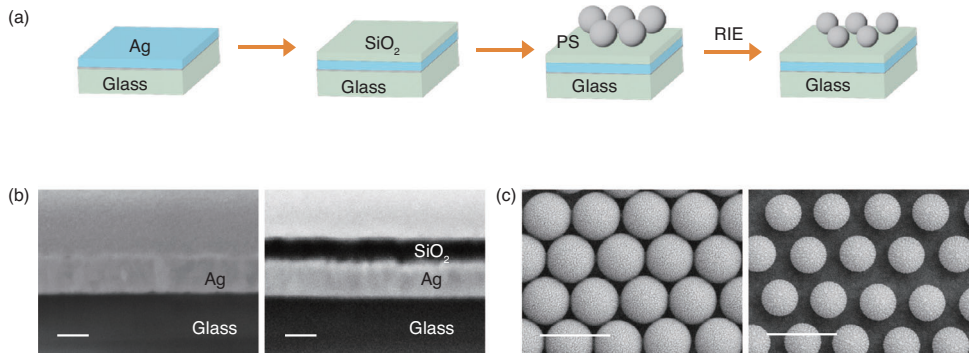

Figure 2. a) Schematic showing the fabrication procedure of SA-PhC slab. b) Scanning electron microscope (SEM) pictures of the substrate cross section corresponding to the fabrication process in (a). Left panel, a 300-nm-thickness Ag film is coated on the glass substrate by using electron beam evaporation (EBE). Right panel, a 200-nm-thickness SiO_2 film is coated on the Ag film by EBE, Scale: 200 nm. c) SEM pictures of the self-assembled PS micro-spheres arrays corresponding to the fabrication process in (a). Left panel, PS micro-spheres are arranged in a hexagonal lattice. Right panel, the diameter of the PS micro-spheres is significantly reduced after using reactive ion etching. Scale: 1 μm.

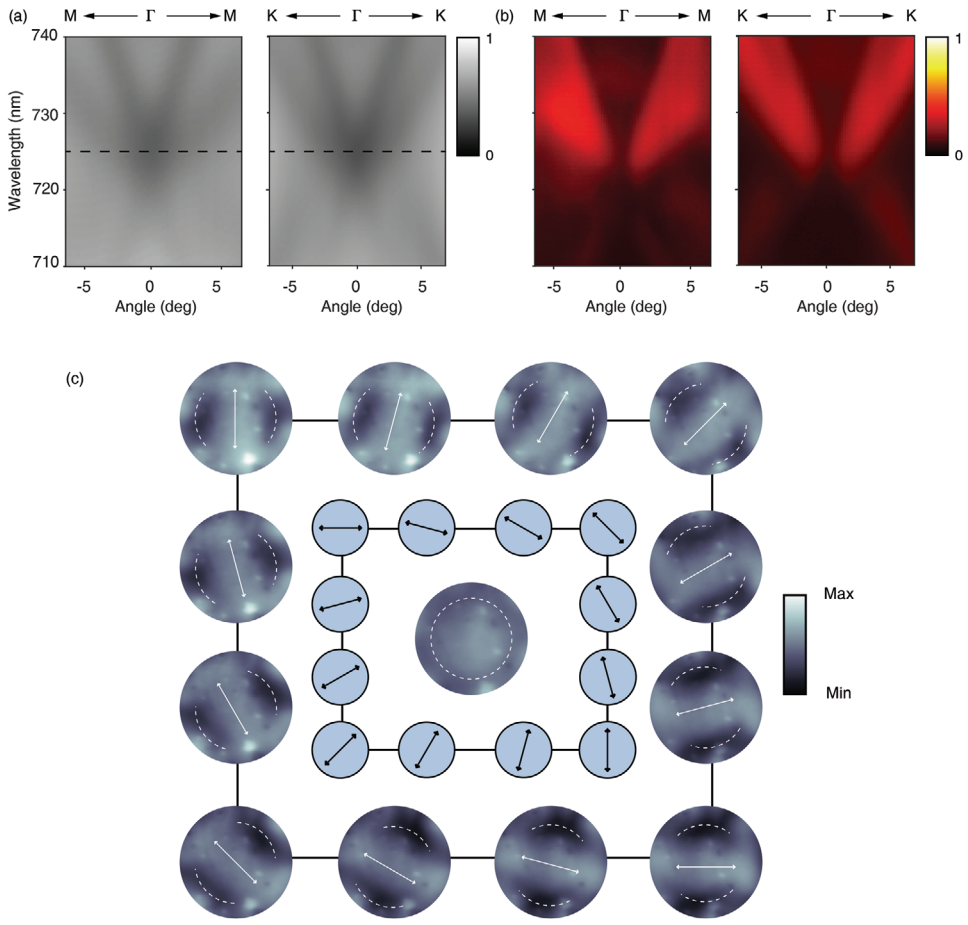

Figure 3. a) Measured angle-resolved reflection spectra along Γ-M and Γ-K direction. b) Measured conversion efficiency along Γ-M and Γ-K direction. c) Experimental verification on vortice polarization behavior in the vicinity of Γ point under narrow-band illumination at wavelengths of 725 nm. The central iso-frequency reflectance profile is measured non-polarized illumination. The studied iso-frequency profile is marked by white-dashed lines. The other iso-frequency reflectance profiles are measured corresponding to polarizer angles, which are marked by black arrows. The diminished regions due to orthogonal polarization are marked with white arrows.

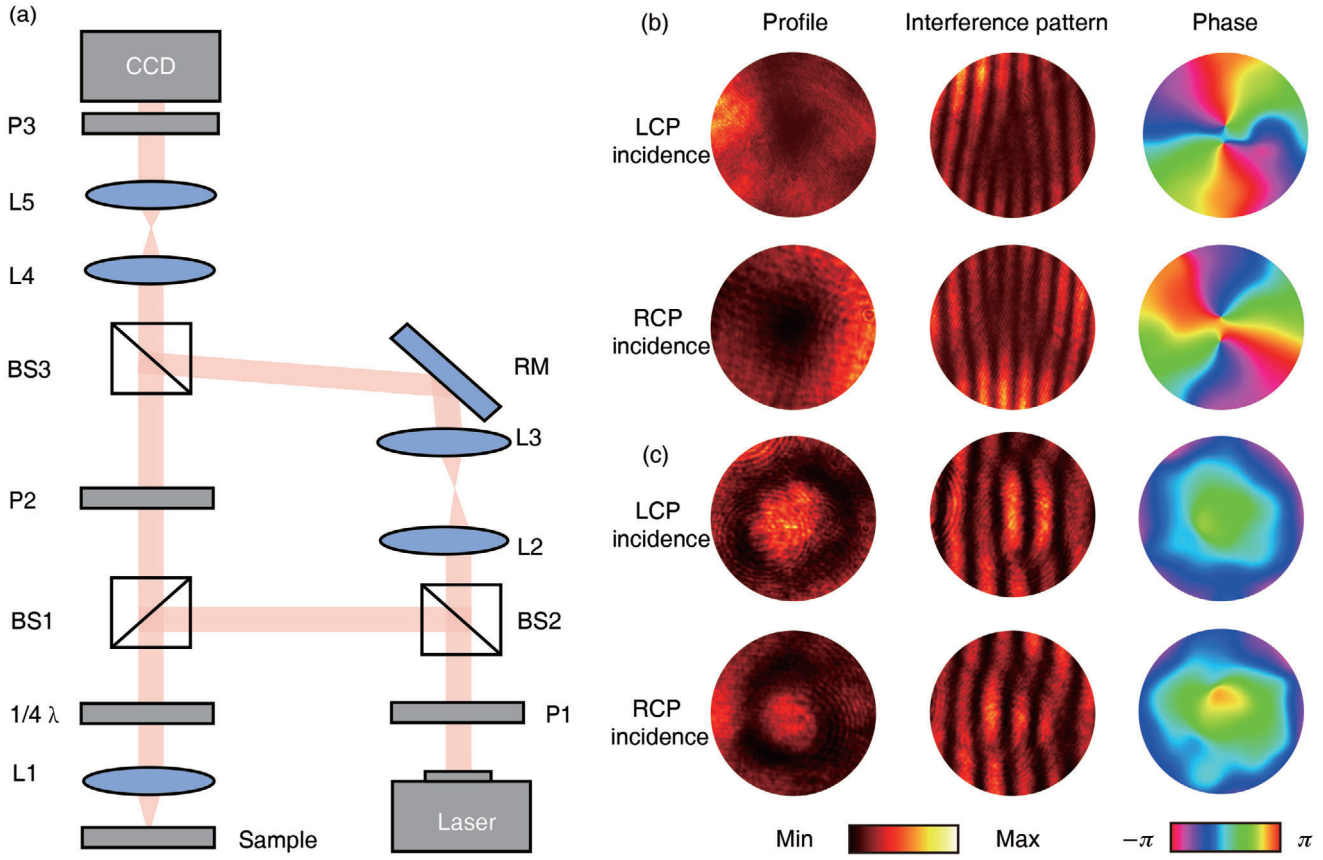

Figure 4. a) The experimental set-up. BS1-BS3, beam splitters; L1–L5, lenses; RM, mirror; P1–P3, polarizers; 1/4λ, quarter-wave plate. b) The measured results of PS micro-spheres array with cross-polarized. From top to bottom, left circularly polarized (LCP) incidence and right circularly polarized (RCP) incidence respectively. Left panel, profiles of the generated wave front. Middle panel, interference patterns between the generated wave front and the inclined coherent planar wave front. Both patterns of cross-polarized wave front have the fork-like dislocation. Right panel, phase distributions of the generated wave front. Both phase distributions of cross-polarized wave front have the spiral phase distribution. c) The measured results of PS micro-spheres array with co-polarized. From top to bottom, LCP incidence and RCP incidence respectively.

nm (see Experimental and Computational Section for more details). As illustrated in Figure 3c, the diminished regions marked by white arrows are indicative of states with SOPs orthogonal to the polarization of the incident beam. As we rotate the polarizer, these diminished regions also rotate, directly demonstrating the vortice behavior. In our measurement, the diminished regions wind along the same direction as that of the polarizer. When the polarizer rotates 2π, the diminished regions also rotate 2π. This indicates the measured polarization vortice carries +1 topological charge. From Equation (2), we can expect the total spiral phase of optical vortice generated by the polarization vortice can be $\pm 4\pi$.

To further characterize OVs profile, we build a home-made reflection-type Fourier-optics-based imaging system. This system features both an imaging mode and an interferometer mode, with the schematic diagram depicted in **Figure** 4a. By removing the reflection mirror in the reference path, the system is initially operated in imaging mode. It measures iso-frequency contours that represent profiles in the far field. In this mode, reference light is not introduced into the measurement. The incident laser is circularly polarized by a circular polarizer module, including a linear polarizer (P1) and a quarter-wave plate (1/4λ), and it is focused on our PS arrays slab through a lens (L1). The focused light, from all directions, impinges upon the PS arrays slab and interacted with k-variant guided resonances surrounding point. Reversely passing through the same lens (L1) and the other circular polarizer module, including 1/4 wave plate (1/4λ) and a linear polarizer (P2), the reflected light is Fourier-transformed into the momentum space. The beam profile is finally detected by charge-coupled device (CCD) after imaging of a set of confocal lenses (L4 and L5). A cross-polarized profile is obtained when the polarization directions of line polarizer P1 and line polarizer P2 are parallel. A co-polarized profile can be obtained when the polarization directions of linear polarizer P1 and linear polarizer P2 are orthogonal. Cross-polarized profiles of LCP and right circularly polarized (RCP) light incidence, co-polarized profiles of LCP and RCP light incidence are plotted in the left panel of Figure 4b,c respectively. It can be seen that the generated cross-polarized beams exhibit doughnut-shaped far-field profiles. However, the co-polarized beams do not have such a characteristic, in the case of co-polarization, no conversion occurs.

Then, we slightly adjust the mirror to introduce a reference light for the interferometer mode. The linearly polarized reference light illuminates the CCD to capture interference patterns between the generated spiral wavefront and the inclined

coherent planar wavefront. The resulting interference patterns are depicted in the corresponding middle panel of Figure 4b,c, respectively. The fork-like dislocation can be found in each profile center interference patterns between the cross-polarized wave front and the reference wave front, and the fork-like dislocation will change their directions, when the circular polarization of incident light is exchanged. But the profile center interference patterns between co-polarized wave front and the reference wave front do not have such a characteristic. Then, we extract phase from the interference patterns, which are plotted in the right panel of Figure 4b,c. The cross-polarized wave fronts both have a spiral phase distribution, but the co-polarized wave fronts have a uniform phase distribution. It could be concluded that the cross-polarized beam with LCP incidence appeared to have a topological charge of +2, while the RCP one had a charge of –2, and co-polarized beams could not generate an OV.

4. Conclusion

In summary, SA-PhC slab was proposed to be able to generate OVs. The OVs generation was demonstrated both in simulations and experiments. The SA-PhC slabs can optimized by modulating the diameter of PS-spheres and adding a SiO_2 spacer. Momentum-space polarization vortices of SA-PhC slab was observed in the fabricated SA-PhC slab. The OVs generation was directly measured and different OVs can be generated by changing the incident circular polarizations. The SA-PhCs have been explored as a low-cost and large-area experimental systems with many applications, and our work offers new application of SA-PhCs in OVs generation. And this new generation methods of via SA-PhC slab can also promote the further applications of OVs.

5. Experimental and Computational Section

Experimental Section: A polarization-resolved momentum-space imaging spectroscopy based on Fourier analysis[42] was used to measure reflectance spectra, conversion efficiency, and iso-frequency contours. An objective was used to perform the optical Fourier transform and obtain the momentum space information on its back focal plane (BFP). Additionally, a white light was focused on the sample by this objective. Then, four achromatic doublet lenses were used followed by the objective to image its BFP on a detector. When reflection spectra and conversion efficiency were measured, a spectrometer was used as the detector. A pair of cross-polarized circular polarizers were added into the setup, conversion efficiency could be attained. When iso-frequence contours were measured, a camera was used as the detector. A narrow-band filter was added in front of the camera to attain the concerned wavelength and a linear polarizer to obtain different polarization directions.

Computational Section: Full-wave electromagnetic simulations were performed using S^4,[43] an open-source program based on rigorous coupled wave analysis (RCWA). It was suitable and efficient for solving periodic structures in the frequency domain. First, the proposed structures were stratified to perform RCWA, and obtain the reflected electromagnetic fields. Then, the data were post-processed to extract the required properties, such as reflection spectra, phase distribution, and conversion efficiency.

Supporting Information

Supporting Information is available from the Wiley Online Library or from the author.

Acknowledgements

This work was supported by Major Program of National Natural Science Foundation of China (Grant No. T2394480,T2394481); National Key R&D Program of China (2023YFA1406900 and 2022YFA1404800); National Natural Science Foundation of China (No. 12234007, No. 12321161645, and No. 12221004); Science and Technology Commission of Shanghai Municipality (22142200400, 21DZ1101500, 2019SHZDZX01 and 23DZ2260100); J. W. is further supported by China National Postdoctoral Program for Innovative Talents (BX20230079) and China Postdoctoral Science Foundation (2023M740721).

Conflict of Interest

The authors declare no conflict of interest.

Data Availability Statement

The data that support the findings of this study are available from the corresponding author upon reasonable request.

Keywords

optical vortices, photonic crystal slabs, polarization vortices in momentum space, self-assembly micro-spheres arrays

Received: January 10, 2024
Revised: March 11, 2024
Published online:

[1] Y. Shen, X. Wang, Z. Xie, C. Min, X. Fu, Q. Liu, M. Gong, X. Yuan, *Light: Sci. Appl.* **2019**, *8*, 90.
[2] K. Y. Bliokh, *Phys. Rev. Lett.* **2006**, *97*, 043901.
[3] C.-C. Lu, H.-Y. Yuan, H.-Y. Zhang, W. Zhao, N.-E. Zhang, Y.-J. Zheng, S. Elshahat, Y.-C. Liu, *Chip* **2022**, *1*, 100025.
[4] X. Ouyang, Y. Xu, M. Xian, Z. Feng, L. Zhu, Y. Cao, S. Lan, B.-O. Guan, C.-W. Qiu, M. Gu, X. Li, *Nat. Photonics* **2021**, *15*, 901.
[5] W. Zhang, X. Jiang, W. Gu, J. Cheng, H. Zhou, J. Dong, D. Huang, X. Zhang, *Chip* **2023**, *2*, 100043.
[6] C. Paterson, *Phys. Rev. Lett.* **2005**, *94*, 153901.
[7] L. Paterson, M. P. MacDonald, J. Arlt, W. Sibbett, P. E. Bryant, K. Dholakia, *Science* **2001**, *292*, 912.
[8] D. G. Grier, *nature* **2003**, *424*, 810.
[9] M. Padgett, R. Bowman, *Nat. Photonics* **2011**, *5*, 343.
[10] X. Li, D. Dan, X. Yu, Y. Zhou, Y. Zhang, W. Gao, M. Li, X. Xu, S. Yan, B. Yao, *Nanophotonics* **2023**, *12*, 4507.
[11] S. Fürhapter, A. Jesacher, S. Bernet, M. Ritsch-Marte, *Opt. Lett.* **2005**, *30*, 1953.
[12] J. Ni, S. Ji, Z. Wang, S. Liu, Y. Hu, Y. Chen, J. Li, X. Li, J. Chu, D. Wu, C.-W. Qiu, *Nat. Photonics* **2023**, *17*, 1.
[13] D. Song, V. Paltoglou, S. Liu, Y. Zhu, D. Gallardo, L. Tang, J. Xu, M. Ablowitz, N. K. Efremidis, Z. Chen, *Nat. Commun.* **2015**, *6*, 6272.
[14] J.-L. Liu, W.-M. Ye, S. Zhang, *Light: Sci. Appl.* **2016**, *5*, e16094.
[15] S. Khonina, V. Kotlyar, M. Shinkaryev, V. Soifer, G. Uspleniev, *J. Mod. Opt.* **1992**, *39*, 1147.
[16] G. A. Turnbull, D. Robertson, G. Smith, L. Allen, M. Padgett, *Opt. Commun.* **1996**, *127*, 183.
[17] L. Marrucci, C. Manzo, D. Paparo, *Phys. Rev. Lett.* **2006**, *96*, 163905.
[18] N. Yu, F. Capasso, *Nat. Mater.* **2014**, *13*, 139.

[19] M. Mehmood, S. Mei, S. Hussain, K. Huang, S. Siew, L. Zhang, T. Zhang, X. Ling, H. Liu, J. Teng, A. Danner, S. Zhang, C.-W. Qiu, *Adv. Mater.* **2016**, *28*, 2533.
[20] C. W. Hsu, B. Zhen, J. Lee, S.-L. Chua, S. G. Johnson, J. D. Joannopoulos, M. Soljačić, *Nature* **2013**, *499*, 188.
[21] B. Wang, W. Liu, M. Zhao, J. Wang, Y. Zhang, A. Chen, F. Guan, X. Liu, L. Shi, J. Zi, *Nat. Photonics* **2020**, *14*, 623.
[22] Y. Zhang, A. Chen, W. Liu, C. W. Hsu, B. Wang, F. Guan, X. Liu, L. Shi, L. Lu, J. Zi, *Phys. Rev. Lett.* **2018**, *120*, 186103.
[23] J. Liu, X. Zhang, W. Li, C. Jiang, Z. Wang, X. Xiao, *Sci. China Mater.* **2020**, *63*, 1418.
[24] Z.-Z. Gu, A. Fujishima, O. Sato, *Chem. Mater.* **2002**, *14*, 760.
[25] P. Jiang, M. J. McFarland, *J. Am. Chem. Soc.* **2004**, *126*, 13778.
[26] X. Zhang, T. Yin, J. Ge, *Adv. Mater.* **2023**, *36*, 2309344.
[27] Y. He, L. Liu, Q. Fu, J. Ge, *Adv. Funct. Mater.* **2022**, *32*, 2200330.
[28] C. Wang, X. Lin, C. G. Schäfer, S. Hirsemann, J. Ge, *Adv. Funct. Mater.* **2021**, *31*, 2008601.
[29] M. Qin, Y. Huang, Y. Li, M. Su, B. Chen, H. Sun, P. Yong, C. Ye, F. Li, Y. Song, *Angew. Chem., Int. Ed.* **2016**, *55*, 6911.
[30] C. Avci, I. Imaz, A. Carné-Sánchez, J. A. Pariente, N. Tasios, J. Pérez-Carvajal, M. I. Alonso, A. Blanco, M. Dijkstra, C. López, D. Maspoch, *Nat. Chem.* **2018**, *10*, 78.
[31] Y. Huang, F. Li, M. Qin, L. Jiang, Y. Song, *Angew. Chem.* **2013**, *125*, 7437.
[32] P. Zhan, Z. Wang, H. Dong, J. Sun, J. Wu, H.-T. Wang, S. Zhu, N. Ming, J. Zi, *Adv. Mater.* **2006**, *18*, 1612.
[33] Z. Wu, J. Li, X. Zhang, J. M. Redwing, Y. Zheng, *Adv. Mater.* **2019**, *31*, 1904132.
[34] M. Hörantner, W. Zhang, M. Saliba, K. Wojciechowski, H. Snaith, *Energy Environ. Sci.* **2015**, *8*, 2041.
[35] Y. S. Zhang, C. Zhu, Y. Xia, *Adv. Mater.* **2017**, *29*, 1701115.
[36] S. G. Romanov, A. V. Korovin, A. Regensburger, U. Peschel, *Adv. Mater.* **2011**, *23*, 2515.
[37] L. Shi, X. Yuan, Y. Zhang, T. Hakala, S. Yin, D. Han, X. Zhu, B. Zhang, X. Liu, P. Törmä, J. Zi, *Laser Photonics Rev.* **2014**, *8*, 717.
[38] M. López-García, J. F. Galisteo-López, Á. Blanco, C. López, A. García-Martín, *Adv. Funct. Mater.* **2010**, *20*, 4338.
[39] J. F. Galisteo-López, M. Lopez-Garcia, C. López, A. García-Martín, *Appl. Phys. Lett.* **2011**, *99*, 8.
[40] B. Zhen, C. W. Hsu, L. Lu, A. D. Stone, M. Soljačić, *Phys. Rev. Lett.* **2014**, *113*, 257401.
[41] T. Li, J. Wang, W. Zhang, X. Wang, W. Liu, L. Shi, J. Zi, *Natl. Sci. Rev.* **2023**, *10*, nwac234.
[42] Y. Zhang, M. Zhao, J. Wang, W. Liu, B. Wang, S. Hu, G. Lu, A. Chen, J. Cui, W. Zhang, C. W. Hsu, X. Liu, L. Shi, H. Yin, J. Zi, *Sci. Bull.* **2021**, *66*, 824.
[43] V. Liu, S. Fan, *Comput. Phys. Commun.* **2012**, *183*, 2233.